Stability of spinning and standing azimuthal modes in symmetric annular chambers: model for transversal forcing

Giulio Ghirardo*[1], Matthew P. Juniper*[1]

[1] Engineering dept., University of Cambridge
* Corresponding author: gg349@cam.ac.uk

This theoretical study investigates spinning and standing modes in azimuthally symmetric annular combustion chambers. Both modes are observed in experiments and simulations, and an existing model predicts that spinning modes are the only stable state of the system (Noiray, Bothien & Schuermans, 2011, Comb. Theory Modelling 15(5) 585–606). We extend this model to take into account the effect that the acoustic azimuthal velocity has on the flames, and propose a phenomenological model based on experiments performed on transversely forced flames. This model contains a parameter, δ, that quantifies the influence that the transversal excitation has on the fluctuating heat release. For small values of δ, spinning modes are the only stable state of the system, while for large values of δ, standing modes are the only stable state. There is also an intermediate range of δ for which both spinning and standing modes are stable.

1 Introduction

Annular combustion chambers usually have a much longer circumference than their length and width, so thermoacoustic oscillations tend to develop in the azimuthal direction. If they travel in a clockwise or anticlockwise direction, with the pressure and velocity nodes travelling at the speed of sound, they are called spinning modes. If the nodes are fixed in space and the wave modulates its amplitude without travelling, they are called standing modes. Both types of mode are found in large eddy simulations (LES), experiments, and real engines. See for example [1] for spinning, [2] for standing, and [3] for both.

Schuermans et al. [4] study an annular combustor as a network of acoustic elements, using a state space representation. Their linear stability analysis predicts that standing modes are linearly unstable. In time, however, these develop into a spinning mode, which they show is the only stable limit-cycle of the system. They show that this behaviour is also seen for a thermoacoustic model containing a one-dimensional wave equation and a nonlinear saturating pressure-dependent heat release. This model is similar to that which will be used in this paper.

Noiray et al. [5] consider the effect of a non-uniform heat-release in the azimuthal direction. If the acoustic mode has azimuthal dependence of the form $\cos(n\theta)$, they show that a non-uniform perturbation of heat release of the form $\cos(2n\theta)$ is particularly influential. The amplitude of this non-uniformity is labelled C_{2n}. For $C_{2n} = 0$, their analysis predicts that only spinning modes are stable. For larger values of C_{2n}, a sum of standing and spinning modes can be stable. Above a critical value of C_{2n}, only standing modes are stable.

This does not explain, however, why stable standing modes are possible in rotationally symmetric configurations with $C_{2n} = 0$, as found by [2, 3]. One explanation could be that combustors create broadband noise, which seems to cause the thermo-acoustic oscillations to switch between different modes [3, 6]. [1, 7] discuss the effect of noise on the system presented in [5], for a symmetric configuration (by setting $C_{2n} = 0$). The only stable states of the system are the two spinning modes. Noise can make the system jump between the two modes, however, and, when it does so, the system passes through the vicinity of a standing mode. Unfortunately this does not explain how, in [2] and in certain configurations of [3], the system has a statistical preference for standing modes.

In summary, current thermoacoustic models cannot explain why standing modes in symmetric annular chambers should be stable, despite experimental evidence that they sometimes are. In this paper we extend the work done in [5], to include the influence of transversal flame excitation and show that a phenomenological model that includes transverse excitation can exhibit stable standing modes as well as stable spinning modes.

2 Setup

The momentum and pressure equation for the fluctuating velocity $\boldsymbol{u}'$ and the fluctuating pressure p', assuming linear acoustics, negligible effects of viscosity and temperature gradients, and a zero[1] Mach number flow, are:

$$\overline{\rho}\frac{\partial \boldsymbol{u}'}{\partial t} + \nabla p' = 0 \tag{1}$$

$$\frac{\partial p'}{\partial t} + \gamma \overline{p} \nabla \cdot \boldsymbol{u}' = \overline{\rho}(\gamma - 1) q' \tag{2}$$

A thorough derivation of these equations can be found in [8]. Since we are interested in the instabilities in the azimuthal direction θ, we write the equations in cylindrical coordinates and, after a suitable nondimensionalization, we obtain

$$\frac{\partial u}{\partial t} + \frac{\partial p}{\partial \theta} = 0 \tag{3}$$

$$\frac{\partial p}{\partial t} + \frac{\partial u}{\partial \theta} = q - \alpha p \tag{4}$$

In these equations all quantities are nondimensional, u is the velocity in the θ direction, q is the heat release, and $\alpha > 0$ is a damping coefficient. Eqn.s (3) and (4) are equivalent to the wave equation, with $\partial q/\partial t$ as a source term:

$$\frac{\partial^2 p}{\partial t^2} + \alpha \frac{\partial p}{\partial t} - \frac{\partial^2 p}{\partial \theta^2} = \frac{\partial q}{\partial t} \tag{5}$$

This model has been the common starting point of [1, 5, 7], and is discussed as well in [4], and more details on the derivation can be found there.

The heat release fluctuations, q, are often assumed to depend either on velocity, pressure, or both, with the inclusion of one or more time delays. However, we start from the analysis of Noiray et al. [5], where q is a function of p only:

$$q = f(p) \tag{6}$$

$$f(p) = \beta p - \kappa p^3 \tag{7}$$

The first term depicts linear growth governed by β for small fluctuating pressures. The second term in (7) is a nonlinear cubic saturation, governed by a coefficient κ. For any given $\kappa > 0$, the

[1] the mean azimuthal velocity is induced only by the swirlers, and is usually negligible

study of eqn. (5) in terms of a new pressure variable $\tilde{p} \equiv p/\sqrt{\kappa}$ leads to a new problem independent of κ. It follows that the coefficient κ induces simply a rescaling of the problem, and will be set to 1 in the following analysis.

The theory developed in [5] based on eqn. (6) does not predict stable standing modes for symmetric configurations, which are observed in [2, 3]. The universal validity of (6) is then called into question, particularly the strong assumptions of (6), which are (i) the absence of a time delay in p and (ii) the independence of q on anything else except p.

Regarding the first point, q has been found to be reasonably in phase with p in a LES simulation of a specific, symmetric rig [2]. In that rig, both standing and spinning modes are observed, suggesting that standing modes are possible in the absence of a time delay. Since the aim of this paper is to explain how standing modes are possible in symmetric systems, we do not consider a time delay and assume that p and q are in phase, leaving this investigation for further research. Some results based on linear stability, applied to an $n-\tau$ model, discussing the importance of the time delay can be found in [9].

Regarding the second point, we can assume, in addition to the dependence of p, a dependence of q on the azimuthal velocity u, which excites transversally the flames. This possibility is investigated in this paper.

3 Model of transversal forcing

The effect of transverse excitation on swirling premixed flames is a current topic of research. Hauser et al. [10] report that an asymmetric perturbation of higher OH intensity is generated by the transversal velocity. This asymmetric region of stronger combustion spirals around the injector at the forcing frequency. This asymmetry persists also in addition to longitudinal forcing, suggesting that the two phenomena are superposable.

Phase averaged chemiluminescence images taken from above an annular combustor by Worth et al. [3] allow us to study, in the presence of standing modes, how the flames interact at pressure nodes and antinodes. At pressure antinodes there is no transverse velocity excitation. Circles of positive/negative heat release are shed from the injector and propagate outwards. The fluctuating heat release is found to be approximately symmetric around the injector: at every instant of time, the phase of the perturbation is approximately axisymmetric. This is consistent with [11], where the vorticity disturbance is symmetric around the injector at pressure antinodes. At velocity antinodes the symmetry of the perturbation breaks: the heat release is found to be approximately in anti-phase on the two sides of the flame, in the direction of the transverse velocity. In [11] the same break of symmetry happens for vortical disturbances, which are asymmetric at velocity antinodes. This means that the spatially averaged heat release fluctuation of an injector is smaller at velocity antinodes. This happens because, in the averaging, the zones in anti-phase cancel out.

Based on this observation, we assume that the fluctuating heat release of an injector is smaller if a transverse excitation is present, introducing a dependence on the velocity u:

$$q(p,u) = f(p)\mu(u) \tag{8}$$

In this expression, f is the same function introduced in (7), and all the previous considerations apply to it. The function μ must be unity for zero transverse excitation, and smaller than 1 for $u \neq 0$, in the range of velocities investigated:

$$0 \leq \mu(u) \leq 1 \ \wedge \ u\frac{\partial \mu}{\partial u}(u) \leq 0 \tag{9}$$

We study two possibilities for μ:

$$\mu(u) = 1 - \delta|u| \qquad \text{Case A} \tag{10}$$

$$\mu(u) = 1 - \delta u^2 \qquad \text{Case B} \tag{11}$$

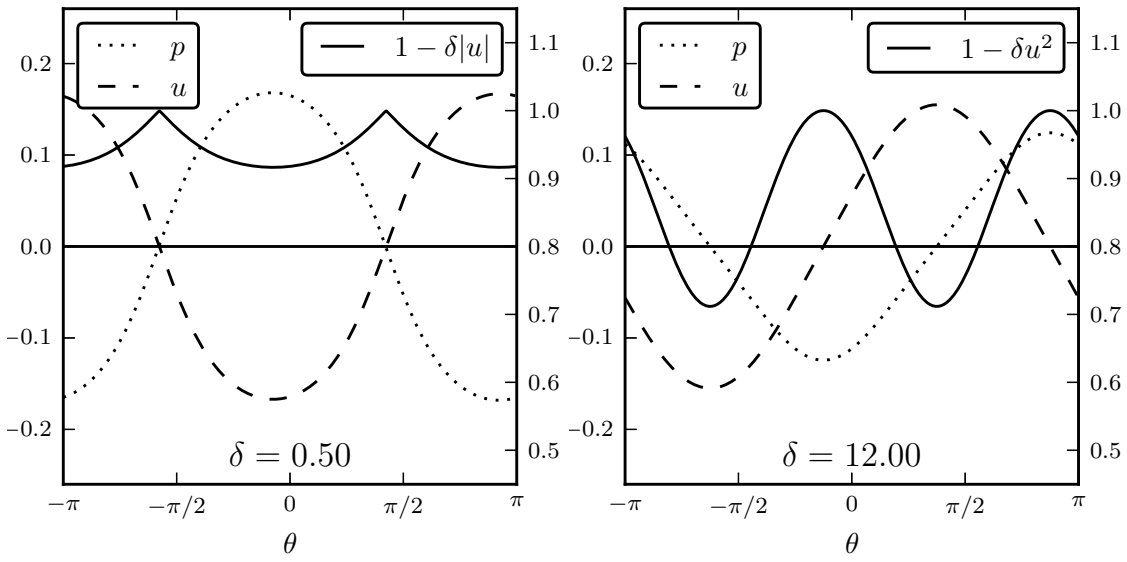

(a) Stable spinning mode

(b) Stable standing mode

Figure 1: Instantaneous snapshots of two simulations, for $\alpha = 0.08, \beta = 0.10$. Pressure and velocity values are reported on the left scale, while $\mu(u(\theta))$ values are reported on the right scale. *a)* μ from case A, $\delta = 1$. The pressure and velocity waves travel either to the left (if in antiphase, as in this case) or to the right (if in phase). δ is small, so the influence of the transverse velocity forcing is small, and the spinning mode is stable. The curve $\mu(\theta)$ also travels left, following the two waves. *b)* μ from case B, $\delta = 12$. The velocity and pressure are standing waves, and their nodes are fixed in space; pressure nodes corresponds to troughs of μ, and velocity nodes correspond to peaks of μ.

with δ a positive coefficient that expresses how strongly the transverse forcing influences the heat release. Both models must respect eqn. (9) at every instant of time.

4 Numerical setup

We opt to study the system of eqn.s (3) and (4), and project them into Fourier space, obtaining a system of ordinary differential equations. The generic n^{th} complex Fourier mode is governed by:

$$\begin{cases} \dot{u}_n &= -inp_n \\ \dot{p}_n &= -inu_n - \alpha p_n + q_n \end{cases} \qquad \forall n = 1, 2, ..., N_f. \tag{12}$$

Since q is a nonlinear function of u and p, at each timestep the two functions $u(\theta)$ and $p(\theta)$ are evaluated from the Fourier coefficients $\{u_n\}$ and $\{p_n\}$, and then $q(\theta)$ is calculated as $f(p(\theta))\mu(u(\theta))$. Finally the $\{q_n\}$ coefficients are evaluated as a Fourier transform of $q(\theta)$. The system (12) can then be numerically integrated with a numerical scheme.

The damping of this problem has to be adjusted to avoid excessive growth of higher order harmonics. Specifically, we consider only the dissipation due to the boundary layers, which scales as the square root of the frequency [8, 12]. We take this into account fixing $\alpha_n = \alpha\sqrt{n}$ in (12).

Two examples of two simulations showing a spinning and a standing mode are reported in figure 1, truncating the number of Fourier modes to $N_f = 161$.

The two pictures do not imply that the two modes are stable, and only time marching for a long time allows us to check this at this stage[2]. We present here both cases A and B only to show

[2]The two modes in the two cases will be proved to be stable later with rigour.

what the two different μ functions defined in (10) and (11) look like. Both cases present spinning modes for small values of δ and standing modes for large values of δ.

The existence of a standing mode at one value of δ and a spinning mode at another is a key result of this paper. In the next sections we conduct a stability analysis of these modes to confirm that they are indeed both stable limit cycles of the nonlinear governing equations.

5 Reduction to a system of coupled oscillators

In this section we carry out spatial averaging in the azimuthal direction, in the same way as [5]. When annular combustors are subject to azimuthal instabilities, there is usually only one strong Fourier component, which corresponds to the n^{th} lowest acoustic mode of the chamber. This is apparent from the power spectral density (PSD) of the Fourier transform of pressure signals from experiments (see for example [3]), and is also observed in the numerical solutions of (12). We truncate the modal expansion and consider only the n^{th} mode:

$$u(t,\theta) = n\eta_1(t)\sin(n\theta) - n\eta_2(t)\cos(n\theta) \tag{13}$$
$$p(t,\theta) = \eta_1'(t)\cos(n\theta) + \eta_2'(t)\sin(n\theta) \tag{14}$$

where the second expression was obtained substituting (13) into (3). We now apply spatial averaging [8] to this system: we substitute (13) and (14) into (4), multiply the expression by $2\cos(n\theta)$, and then average over 2π in the azimuthal coordinate, obtaining (15):

$$\eta_1'' + \alpha\eta_1' + n^2\eta_1 = F_1 \tag{15}$$
$$\eta_2'' + \alpha\eta_2' + n^2\eta_2 = F_2 \tag{16}$$

Here, (16) has been obtained similarly by multiplying by $2\sin(n\theta)$. Notice that these expressions are exact, and the assumption that higher order modes are negligible is applied assuming that the two source terms on the RHS depend only on the Fourier modes η_1 and η_2. These two terms are:

$$F_1 = \frac{1}{\pi}\int_0^{2\pi} q\Big(\eta_1'\cos(n\theta) + \eta_2'\sin(n\theta), n\eta_1\sin(n\theta) - n\eta_2\cos(n\theta)\Big)\cos(n\theta)d\theta \tag{17}$$
$$F_2 = \frac{1}{\pi}\int_0^{2\pi} q\Big(\eta_1'\cos(n\theta) + \eta_2'\sin(n\theta), n\eta_1\sin(n\theta) - n\eta_2\cos(n\theta)\Big)\sin(n\theta)d\theta \tag{18}$$

We can study the system in the new timescale $t' = nt$, and obtain:

$$\eta_1'' + \alpha\eta_1' + \eta_1 = f_1(\eta_1, \eta_2, \eta_1', \eta_2') \tag{19}$$
$$\eta_2'' + \alpha\eta_2' + \eta_2 = f_2(\eta_1, \eta_2, \eta_1', \eta_2') \tag{20}$$

where we dropped for ease of notation the prime from t', we substituted $\alpha \longmapsto \alpha/n$, and the expressions for f_i are $f_i \equiv F_i/n^2$. This is a system of coupled oscillators, which can be numerically integrated in time in a 4-dimensional phase space, as opposed to the phase space with N_f dimensions introduced in (12).

mode	Amplitudes and phase	Trajectory in the plane (η_1, η_2)
spinning	$\theta = \pm\pi/2$ with $A = B$,	circle
standing	$\theta = 0 \vee \pi$ with arbitrary A, B	line with arbitrary inclination

Table 1: Characterization of spinning and standing modes

5.1 Amplitudes and phase representation

Instead of studying the system in terms of displacements, η_i, and velocities, $\dot{\eta}_i$, it is more useful to study it in terms of amplitudes and phases,

$$\eta_1(t) = A(t)\cos(\omega t + \varphi_1(t)) \tag{21}$$
$$\dot{\eta}_1(t) = -A(t)\omega\sin(\omega t + \varphi_1(t)) \tag{22}$$
$$\eta_2(t) = B(t)\cos(\omega t + \varphi_2(t)) \tag{23}$$
$$\dot{\eta}_2(t) = -B(t)\omega\sin(\omega t + \varphi_2(t)) \tag{24}$$

In these expressions, $\omega = 1 + \mathcal{O}(\beta)$, where 1 is the natural frequency of both oscillators. Eqn.s (19) and (20) are symmetric in η_1, η_2. It is useful to introduce the phase difference between the two oscillators, $\theta(t) \equiv \varphi_1(t) - \varphi_2(t)$. If θ settles to $\pm\pi/2$ and $A = B$, then the substitution of (22) and (24) into (14) shows that the pressure distribution corresponds to a spinning mode in the counterclockwise/clockwise direction respectively:

$$p(t, \theta) = -A\omega\sin(\omega t + \varphi_1 \mp n\theta) \tag{25}$$

This solution spins in the azimuthal direction as in Figure (1.a). On the other hand, if θ settles to π or 0, there is a standing mode, for any value of A, B:

$$p(t, \theta) = \omega\sin(\omega t + \varphi_1)(-A\cos(n\theta) \pm B\sin(n\theta)) \tag{26}$$

The pressure nodes can be found by studying the zeros of the θ-term in (26). They are fixed in space, as shown in Figure (1.b). It is convenient to examine the two cases in the (η_1, η_2) plane as a function of time. With reference to eqn.s (21-24), the two modes give rise to limit-cycles which are either circles or lines. The situation is summarized in table 1. Figure 2 shows two simulations of trajectories in the (η_1, η_2) plane for case B. The two cases have different values of δ, and lead to either spinning or standing limit-cycles. The simulations have been started with nearly the same initial condition for θ, and from two random values for A, B.

6 Stability of the coupled oscillator system

We first report some results from the linear analysis of the fixed point $p(t, \theta) = u(t, \theta) = 0$ of the system (19,20). This fixed point is stable for $\beta < \alpha$. A double Hopf bifurcation occurs at $\beta = \alpha$, where two complex eigenvalues cross the imaginary axis at the same time. Similarly, [9] perform a linear stability analysis of an azimuthally symmetric chamber and find two linearly unstable spinning modes with exactly the same growth rate. They conclude that, in perfectly symmetric systems, the sum of the two identical spinning modes would lead to a stable standing mode. This is not the case, however, as shown by the fact that, for $\delta = 0$, and $\beta > \alpha$, this system converges to a stable spinning mode, in accordance with [4].

We proceed by analysing the case of the oscillating system, fixing $\alpha = 0.08$ and $\beta = 0.10$, and focusing on case A. Figure 2 shows that two different values of δ lead to two different limit cycles: a spinning mode and a standing mode. We now study the system over a range of δ. To do this, we numerically integrate the system until it converges to a limit cycle, and then track the limit cycle as we vary δ using MatCont, a numerical continuation package [13]. Figure 3 shows the

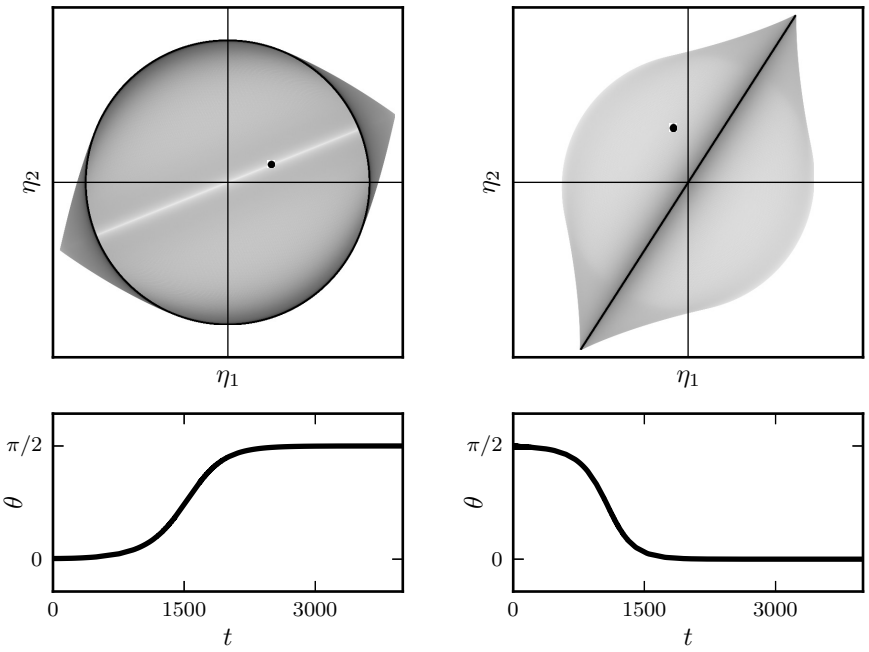

(a) $\delta = 3$. Transition to a spinning mode (b) $\delta = 12$. Transition to a standing mode

Figure 2: Temporal evolution to stable limit cycles, for two different values of δ. In both simulations, $\alpha = 0.08, \beta = 0.10$, and μ is from case B. The top plots show the trajectory of the system in the (η_1, η_2) plane; The black dot is the initial position and the darkness of the line is proportional to the simulation time t. In this plane, spinning modes are circles around the origin, and standing modes are lines centred on the origin, at an arbitrary angle that depends only on the initial conditions. In the left frames, the spinning mode is stable. In the right frames, the standing mode is stable. The bottom plots show the temporal evolution of the phase θ between the two oscillators. The values of θ can be compared with those in table 1.

stability of the spinning and standing modes. For $\delta = 0$, the spinning mode is stable, because all its Floquet multipliers are smaller than 1 in Figure 3.a. At $\delta_{c2} \approx 1.027$, the modulus of two Floquet multipliers crosses 1, which corresponds to a subcritical[3] Neimark-Sacker bifurcation at which the spinning mode becomes unstable. The argument of these two Floquet multipliers, shown in Figure 3.c, is small. Notice that, for $\delta > \delta_{c2}$, there is one multiplier with modulus smaller than 1 and two multipliers with modulus greater than 1. This means that the system is attracting from an invariant manifold[4] with dimension 1, and repelling to another invariant manifold with dimension 2. This is consistent with figure 2.b, where the point is first attracted to the spinning mode (circular line) before being repelled towards a standing mode (straight line).

For the standing mode, for every value of δ, two multipliers are exactly equal to 1. One of these is due to the fact that the system is at a limit-cycle and any movement in the direction of the limit cycle remains on the limit cycle (the spinning mode has one too, under the horizontal black line in figure 3.a). The other is due to the fact that the nodes of the standing mode can rotate arbitrarily around the annulus - i.e. the black line in figure 2.b can take any angle with the axes.

[3] based on the first Lyapunov exponent, which is positive

[4] for the purposes of this article, an invariant manifold can be thought of as a particular surface in the phase space such that all points on it are either attracted to or repelled from the same limit-cycle or fixed point. Refer to [14] for a rigorous definition.

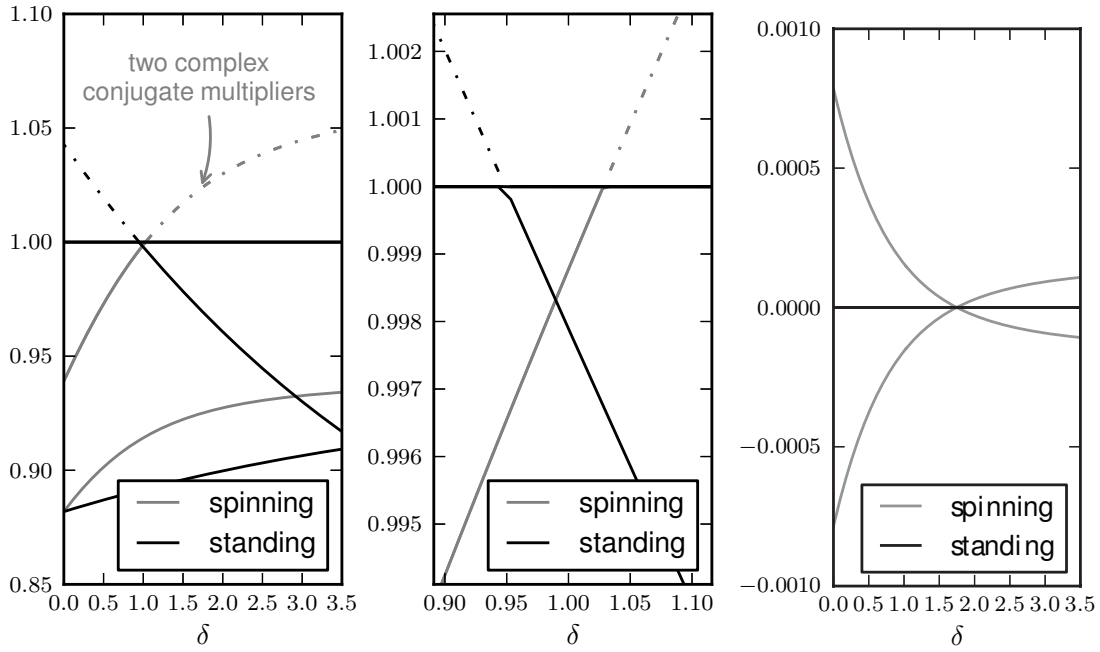

(a) Modulus of the Floquet multipliers

(b) Zoom of Figure (a))

(c) argument of the Floquet multipliers

Figure 3: Stability of standing and spinning limit-cycles with respect to the transversal forcing parameter δ. (a) Modulus of the Floquet multipliers of both modes. To each multiplier corresponds an invariant manifold on which the system is attracted towards the limit-cycle if the modulus is smaller than 1 (continuous lines) or repelled from the limit-cycle if the modulus is larger than 1 (dashed lines). One limit-cycle is unstable if there is at least one multiplier larger than 1. From (a), for small values of δ only the spinning mode is stable, and for large values of δ only the standing mode is stable. The standing limit cycle has two coincident multipliers equal to 1, while the spinning limit cycle has only one multiplier equal to 1 (not visible, covered by the black line) and a couple of complex conjugate multipliers (indicated with the arrow). From the zoom in (b), we observe there is a range of δ where both modes are stable. (c) Argument of the Floquet multipliers, which is needed to discuss the type of bifurcation at criticality. The two non-zero arguments of the spinning mode belong to the complex conjugate pair presented in (a).

A fold bifurcation occurs at $\delta_{c1} = 0.949$, making the mode stable for $\delta > \delta_{c1}$. Notice that, for $\delta < \delta_{c1}$, there is one multiplier with modulus smaller than 1 and one multiplier larger than 1. This means that the system is attracting from a 1-dimensional invariant manifold and repelling from another 1-dimensional invariant manifold. This can be seen in Figure 2.a, where for a while the solution lingers as a standing mode (straight line) before being repelled towards the spinning mode (circle line).

The angular frequency of the limit cycles is not changed by the nonlinearities of the problem: in the range of parameters investigated, the period of oscillations was found to be constant and equal to 2π. In summary:

- for $\delta < \delta_{c1} \approx 0.949$ only the spinning mode is stable;
- for $\delta > \delta_{c2} \approx 1.027$ only the standing mode is stable;
- for $\delta_{c1} < \delta < \delta_{c2}$, the system is multistable, with both standing and spinning modes stable.

Moreover, for $\delta < \delta_{c1}$ and $\delta > \delta_{c2}$ the unstable mode attracts the solution on a 1-dimensional invariant manifold, before repelling it towards the stable mode.

We checked that these stability results, obtained for the system (19,20), apply also to the original system (5) by performing numerical simulations of (12) for different values of δ. For each value of δ, we started the simulation with both standing and spinning modes as initial conditions, and evaluated their stability by time-marching. The same qualitative picture was found, with the two critical values of δ confined in these intervals: $0.9 < \delta_{c1} < 1.0$, and $1.1 < \delta_{c2} < 1.2$, in good agreement with the values just presented. This shows that the reduction to a system of coupled oscillators by considering only the fundamental unstable harmonic, as presented in section 5, is a powerful tool to study the stability of the original wave eqn. (5), at least at the moderate value of $\beta - \alpha$ here investigated.

We do not report here the analysis for case B, because it presents the same overall behaviour of case A.

7 Slow flow

In this section we apply the method of averaging to the system of coupled oscillators (19,20) for case B. We will obtain a new system of differential equations in terms of the amplitudes of oscillation A, B and of the phase difference θ, introduced from eqn. (21) onwards. This will reduce the dimensions of the problem from 4 to 3, allowing us to visualize the complete dynamics of the problem. The method of averaging [15] gives the following formulation of the slow flow:

$$\begin{cases} A' = & \frac{\alpha}{2} A - \langle s_1 f_1 \rangle \\ B' = & \frac{\alpha}{2} B - \langle s_2 f_2 \rangle \\ \omega\theta' = & -\frac{1}{A}\langle c_1 f_1 \rangle + \frac{1}{B}\langle c_2 f_2 \rangle \end{cases} \tag{27}$$

where $s_i \equiv \sin(\omega t + \varphi_i)$ and $c_i \equiv \cos(\omega t + \varphi_i)$, and the averaging operator of a generic function h is introduced as

$$\begin{aligned} \langle h(\eta_1, \dot{\eta}_1, \eta_2, \dot{\eta}_2) \rangle \equiv \frac{\omega}{2\pi} \int_t^{t+\frac{2\pi}{\omega}} h\Big(& A\cos(\omega t + \varphi_1), \\ & -A\omega \sin(\omega t + \varphi_1), \\ & B\cos(\omega t + \varphi_2), \\ & -B\omega \sin(\omega t + \varphi_2) \Big) dt, \end{aligned} \tag{28}$$

and we do not report here the full expressions of (27). Notice that, while in the definitions (21-24) the amplitudes and the phases are functions of time, they are constants in the RHS of (28). We fix $\omega = 1$, consistently with the period being 2π as reported earlier.

We leave a full characterization of the stability of the system (27) as a function of $\alpha, \beta, \delta, \kappa$ to future research. We fix the values of $\kappa = 1, \alpha = 0.08, \beta = 0.1$, and draw the phase space for $\delta = 3$ (spinning mode) and for $\delta = 12$ (standing mode). The amplitudes A, B are non-negative numbers, and $\theta \in [0\,,\, 2\pi]$. Since the phase space is symmetric with respect to the planes $\theta = k\pi/2$ with $k = 0, 1, 2$, we restrict the visualization to $\theta \in [\pi/2\,,\, \pi]$. The system is also symmetric with respect to the plane defined by $A = B$.

Because of the difficulty of drawing a 3 dimensional phase space, we report the flow on a few invariant manifolds. These completely describe the stability of the problem[5]. Figure 4 shows two convenient slices of the same phase space for $\delta = 3$. In the picture, every shaded surface is an invariant manifold, and all invariant manifolds are reported, with the exception of the two planes $A = 0$ and $B = 0$. In Figure 4, the spinning mode is stable, because $\delta < \delta_c$. We then fix $\delta = 12 > \delta_c$ and present the same slices of the phase space in Figure 5, in which the standing mode is stable.

[5] The flow perpendicular to an invariant manifold is zero

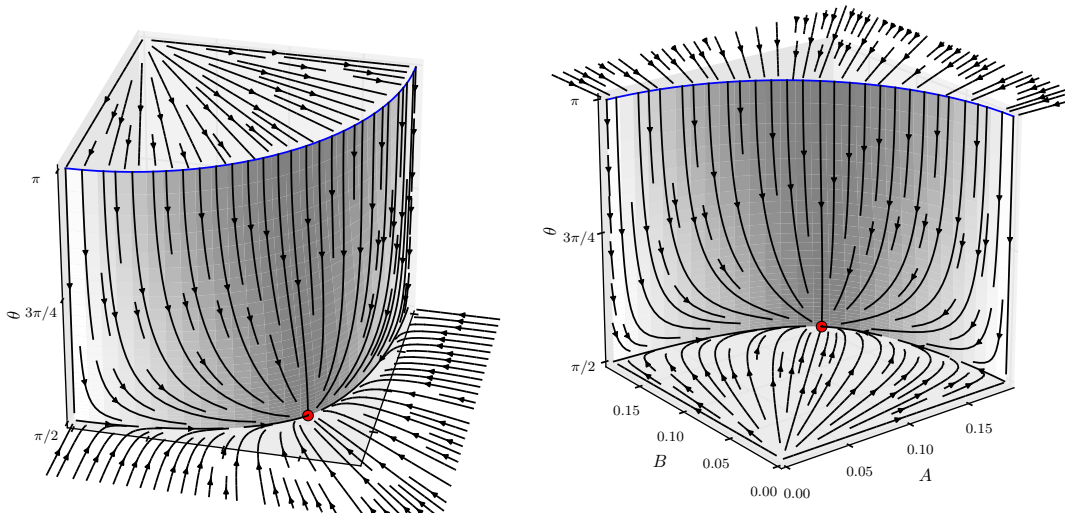

(a) Front view

(b) Back view

Figure 4: Two views of the 3D phase space, in terms of the amplitudes A and B of the two modes and of the phase θ between them. $\delta = 3 < \delta_{crit}$. The line $A = B = 0$ corresponds to the trivial solution with zero pressure and velocity in the whole domain. The three surfaces are invariant manifolds and the direction of the local vector field, which is tangential to them, is described by the arrows. The spinning mode is reported as a red dot, and the standing mode as a blue arc. For this value of δ, the spinning mode is stable and the standing mode is unstable. The phase space is symmetric with respect to the plane $\theta = \pi$, with the image of the red dot under symmetry indicating a spinning mode with the opposite azimuthal direction.

In this representation, the addition of a non-zero asymmetry parameter, C_{2n}, as proposed in [5], shifts the red point of Figure 4 towards one of the A, B axes, maintaining it on the same plane $\theta \pm \pi/2$. Doing so, the system exhibits a superposition of standing and spinning modes. As discussed in [5], above a certain threshold the red point hits and gets stuck on one of the A, B axes, becoming a pure standing mode. The current analysis shows that, with the addition of transverse forcing introduced in (8), with $\mu(u)$ from case B as defined in (11), the standing mode becomes stable in a different way, without passing through a superposition of standing and spinning modes.

8 Conclusions

This study improves the current understanding of standing and spinning modes in symmetric annular combustion chambers, which is the subject of current research [2–4, 7, 9]. The starting point of this study is the model proposed in [5]: the fluctuating heat release q is assumed to grow linearly and saturate nonlinearly as the pressure increases, as $q = f(p) = \beta - \kappa p^3$. In our analysis, we add an extra dependence, which reflects experimental observations [3, 10]: the fluctuating heat release fluctuates axisymmetrically at velocity nodes (pressure antinodes), while it fluctuates from side to side at velocity antinodes (pressure nodes). When integrated over a sector of the chamber, the q fluctuations are larger in the first case. We then assume that $q = f(p)\mu(u)$, and we study two ways in which q can depend on u. We consider a case A with $\mu(u) = 1 - \delta|u|$, and a case B with $\mu(u) = 1 - \delta u^2$.

For both cases, we find that: (i) for small δ, only spinning modes are stable; (ii) for intermediate δ, both standing and spinning modes are stable, and the system is multistable; (iii) for large δ,

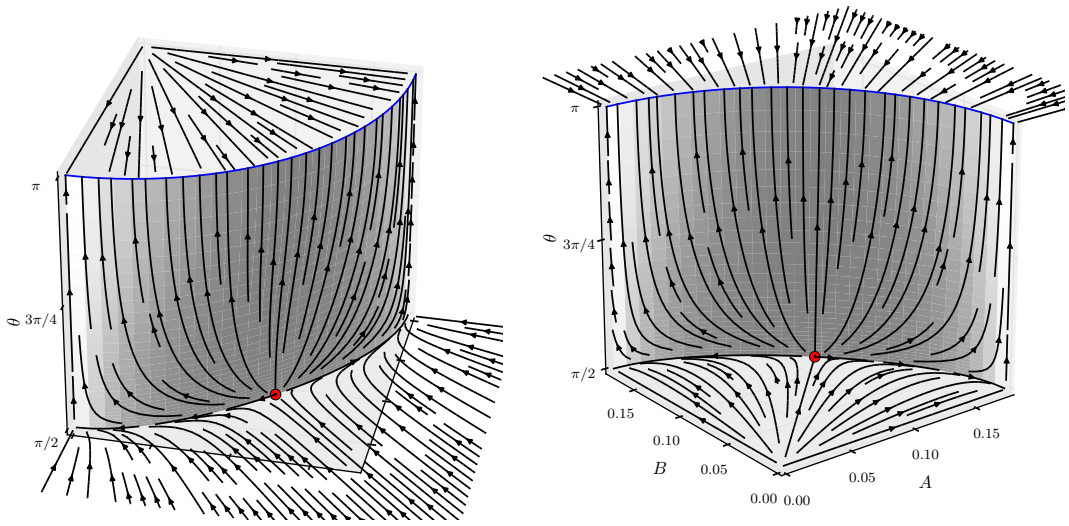

(a) Front view

(b) Back view

Figure 5: Two views of the same 3D phase space with $\delta = 12 > \delta_{crit}$. In comparison with figure 4, there is now a change of direction of the arrows on the nonplanar surface. For this value of δ the standing modes (blue arc) are now stable, and the spinning mode (red dot) is unstable.

only standing modes are stable.

Another result is that, when the system has only one stable limit-cycle, the other unstable limit-cycle is not a repellor: it attracts the solution on one invariant manifold, and repels it on another. Figure 12 in [4] suggests that the same property applies also to their system. If this property holds in industrial combustors, noise could randomly shift the point in the phase space also to the attracting manifold of the unstable mode, and the system could linger for longer close to the unstable mode before decaying to the stable one. We give an example of this transient behaviour in figure 2, and we comment on it based on the stability results in section 6.

This work suggests that transversal forcing plays an important role in annular combustion instabilities, and should be taken into account to accurately predict instabilities in annular configurations. The experimental characterization of a single injector to longitudinal forcing seems to not be sufficient to predict the final state of the combustor.

References

[1] N. Noiray and Bruno Schuermans. Azimuthal thermoacoustic modes in annular gas turbine combustion chambers. *ICSV19 conference, Lithuania*, 2012.

[2] P. Wolf, G. Staffelbach, L. Y. M. Gicquel, J. D. Müller, and T. Poinsot. Acoustic and Large Eddy Simulation studies of azimuthal modes in annular combustion chambers. *Combustion and Flame*, 159(11):3398–3413, November 2012.

[3] N. A. Worth and James R. Dawson. Self-excited circumferential instabilities in a model annular gas turbine combustor: Global flame dynamics. *Proceedings of the Combustion Institute*, 34(2):3127–3134, January 2013.

[4] B. Schuermans, C. O. Paschereit, and P. A. Monkewitz. Non-linear Combustion Instabilities in annular gas-turbine combustors. *44th AIAA Aerospace Sciences meeting and Exhibit*, 2006.

[5] N. Noiray, M. Bothien, and B. Schuermans. Investigation of azimuthal staging concepts in annular gas turbines. *Combustion Theory and Modelling*, 15(5):585–606, October 2011.

[6] T. Poinsot, P. Wolf, G. Staffelbach, L. Y. M. Gicquel, and J. D. Muller. Identification of azimuthal modes in annular combustion chambers. *Annual research briefs. Center for Turbulence Research.*, pages 249–258, 2011.

[7] N. Noiray and B. Schuermans. On the dynamic nature of azimuthal thermoacoustic modes in annular gas turbine combustion chambers. *Proc. R. Soc. A*, 469, 2013.

[8] F. E. C. Culick. *Unsteady Motions in Combustion Chambers for Propulsion Systems*, volume 323. NATO Research and Technology Organization, 2006.

[9] C. Sensiau, F. Nicoud, and T. Poinsot. A tool to study azimuthal standing and spinning modes in annular combustors. *International Journal of Aeroacoustics*, 8(1-2), 2009.

[10] M. Hauser, M. Lorenz, and T. Sattelmayer. Influence of Transversal Acoustic Excitation of the Burner Approach Flow on the Flame Structure. *Journal of Engineering for Gas Turbines and Power*, 133(4):041501, 2011.

[11] J. O'Connor and T. C. Lieuwen. Further characterization of the disturbance field in a transversely excited swirl stabilyzed flame. *Proceedings of the ASME TurboExpo 2011*, 183(5), 2011.

[12] L. D. Landau and E.M. Lifshitz. *Fluid mechanics, 2nd edition.* Pergamon press, 1978.

[13] A. Dhooge, W. Govaerts, and Yu A. Kuznetsov. Matcont : A Matlab package for numerical bifurcation analysis of ODEs. *Transactions on Mathematical Software*, 29(2):141–164, 2003.

[14] J. Guckenheimer and P Holmes. *Nonlinear oscillations, dynamical systems, and bifurcations of vector fields.* 1983.

[15] J.A. Sanders, F. Verhulst, and J. Murdock. *Averaging methods in nonlinear dynamical systems*, volume 59. Springer, 2nd edition, 2007.